# ADVANCED MATERIALS

## Supporting Information

Molecular Alignment of Homoleptic Iridium Phosphors in Organic Light-Emitting Diodes

*Moon Chul Jung, John Facendola, Jongchan Kim, Daniel Sylvinson Muthiah Ravinson, Peter I. Djurovich, Stephen R. Forrest, and Mark E. Thompson\**

# Molecular Alignment of Homoleptic Iridium Phosphors in Organic Light-Emitting Diodes.

Moon Chul Jung[1], John Facendola[2], Jongchan Kim[3], Daniel Sylvinson Muthiah Ravinson[2], Peter I. Djurovich[2], Stephen R. Forrest[3,4], Mark E. Thompson[1,2]*

1. Mork Family Department of Chemical Engineering and Materials Science, University of Southern California, Los Angeles, California 90089, United States

2. Department of Chemistry, University of Southern California, Los Angeles, California 90089, United States

3. Department of Electrical and Computer Engineering, University of Michigan, Ann Arbor, Michigan 48109, United States

4. Department of Physics and Materials Science and Engineering, University of Michigan, Ann Arbor, Michigan 48109, United States
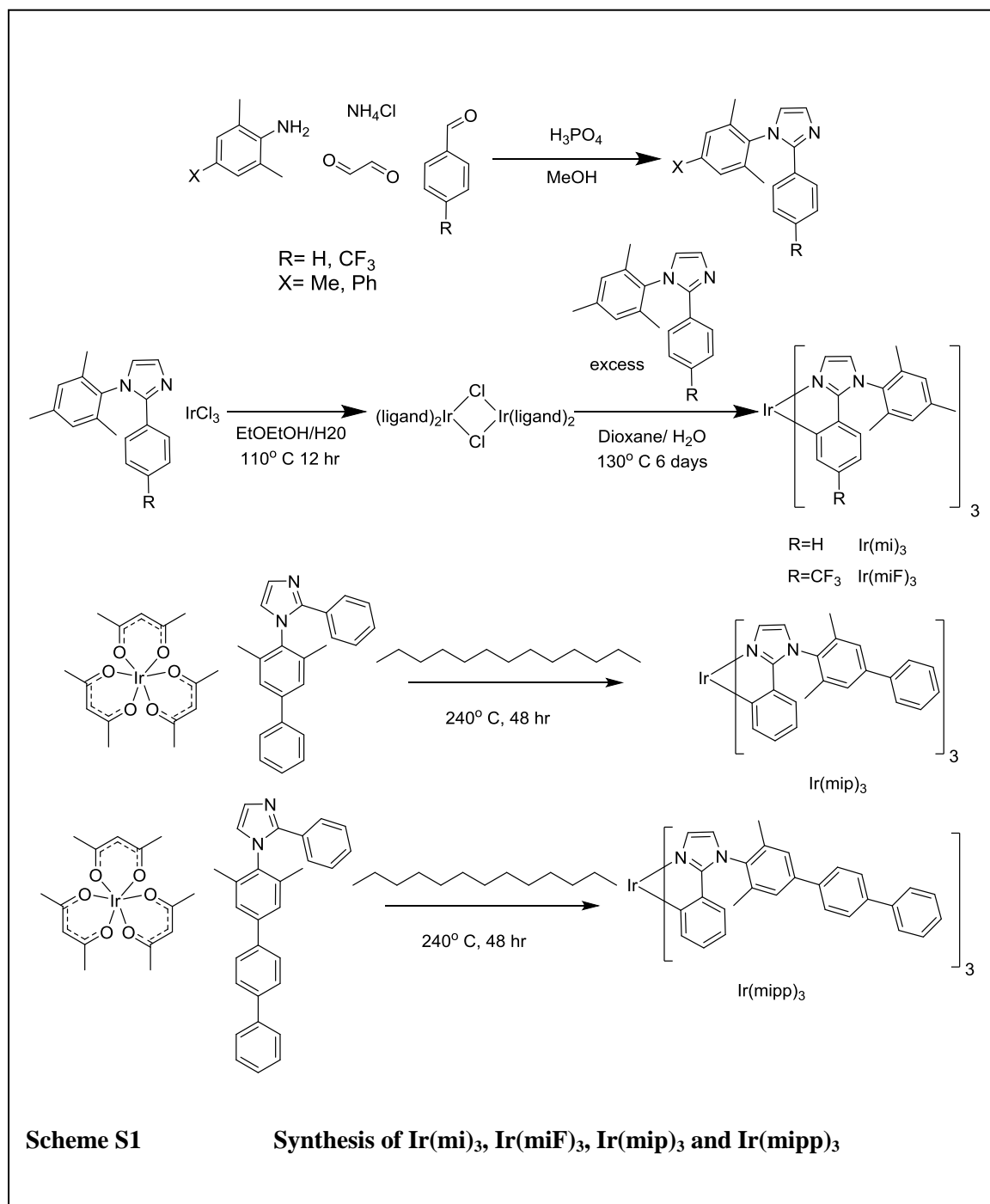
Email: met@usc.edu

# Contents

**Synthesis**



**Scheme S1**          **Synthesis of Ir(mi)₃, Ir(miF)₃, Ir(mip)₃ and Ir(mipp)₃**

All reagents and solvents were received from commercial sources such as Sigma Aldrich. All complexation procedures were carried out in inert $N_2$ gas atmosphere despite the air stability of the complexes, the main concern being the oxidative and thermal stability of intermediates at the high temperatures of the reactions. Both the $[(mi)_2IrCl]_2$ and

4

[(miF)$_2$IrCl]$_2$ dimers were synthesized by the Nonoyama method which involves heating IrCl$_3$·H$_2$O to 110 °C with 2−2.5 equivalents of mi-H and miF-H in a 3:1 mixture of 2-ethoxyethanol and deionized water.[1] Ir(ppy)$_3$, Ir(ppyCF$_3$)$_3$ Ir(mi)$_3$ were prepared according to the literature procedure.[2] Except for Ir(mipp)$_3$, three compounds sublime with the reasonable yields (>50%), allowing for them to be employed in OLEDs.

**1-mesityl-2-phenyl-1H-imidazole (mi-H).** A three neck flask was charged with 2,4,6-trimethylaniline (10.0 g, 74 mmol), glyoxal (10.73 g, 74.0 mmol) and 125 mL of methanol. The reaction mixture stirred at room temperature for 20 hours, upon which benzaldehyde (7.85 g, 74 mmol) and ammonium chloride (3.96 g, 74 mmol). A condenser was attached and the reaction was heated to reflux. Phosphoric acid (724 mg, 7.4 mmol) was added after one hour and the reaction was left to reflux for an additional 24 hrs. The reaction was cooled to ambient temperature and concentrated *in vacuo* to remove the methanol solvent. The crude mixture was diluted with ethyl acetate and treated with 1 M aqueous sodium hydroxide solution. The layers were then extracted and separated with water three times, and the resultant organic layer was then washed with brine, dried with sodium sulfate and concentrated *in vacuo*. The crude mixture was further purified by column chromatography (4:1 hexanes:ethyl acetate) to yield a pale yellow solid (1.67 g, 8.6%). $^1$H NMR (400 MHz, CDCl$_3$ $\delta$) 7.41 − 7.37 (m, 2H), 7.29 (d, $J$ = 1.2 Hz, 1H), 7.22 − 7.17 (m, 3H), 6.94 (d, $J$ = 0.7 Hz, 2H), 6.86 (d, $J$ = 1.2 Hz, 1H), 2.33 (s, 3H), 1.90 (d, $J$ = 0.6 Hz, 6H).

**1-mesityl-2-(4-(trifluoromethyl)phenyl)-1H-imidazole (miF-H).** A three neck flask was charged with 2,4,6-trimethylaniline (7.00 g, 51.8 mmol), glyoxal (7.51 g, 51.8 mmol) and 125 mL of methanol. The reaction mixture stirred at room temperature for 20 hours, upon which 4-(trifluoromethyl)benzaldehyde (9.01 g, 51.8 mmol) and ammonium chloride (2.77 g, 51.8 mmol). A condenser was attached and the reaction was heated to reflux. Phosphoric acid (507 mg, 5.18 mmol) was added after one hour and the reaction was left to reflux for an additional 24 hrs. The reaction was cooled to ambient temperature and concentrated *in vacuo* to remove the methanol solvent. The crude mixture was diluted with ethyl acetate and treated with 1 M aqueous sodium hydroxide solution. The layers were then extracted and separated with water three times, and the resultant organic layer was then washed with brine, dried with sodium sulfate and concentrated *in vacuo*. The crude mixture was further purified by column

chromatography (4:1 hexanes:ethyl acetate) to yield a pale yellow solid (1.56 g, 9.3%). ^{1}H NMR (400 MHz, Acetone-d6) $\delta$ 7.64 − 7.57 (m, 4H), 7.31 (d, $J$ = 1.2 Hz, 1H), 7.18 (d, $J$ = 1.2 Hz, 1H), 7.08 (m, 2H), 2.35 (s, 3H), 1.90 (s, 6H). Elemental Analysis: Anal. Cacld. for $C_{19}H_{17}F_3N_2$: C, 69.08 %; H, 5.19 %; N, 8.48 %. Found: C, 69.27 %; H, 5.55 %; N, 8.71 %

**1-(3,5-dimethyl-[1,1'-biphenyl]-4-yl)-2-phenyl-1H-imidazole (mip-H).** A three neck flask was charged with 3,5-dimethyl-[1,1'-biphenyl]-4-amine (5.00 g, 25.3 mmol), glyoxal (3.68 g, 25.3 mmol) and 100 mL of methanol. The reaction mixture stirred at room temperature for 20 hours, upon which benzaldehyde (2.69 g, 25.3 mmol) and ammonium chloride (1.36 g, 25.3 mmol). A condenser was attached and the reaction was heated to reflux. Phosphoric acid (248 mg, 2.53 mmol) was added after one hour and the reaction was left to reflux for an additional 24 hrs. The reaction was cooled to ambient temperature and concentrated *in vacuo* to remove the methanol solvent. The crude mixture was diluted with ethyl acetate and treated with 1 M aqueous sodium hydroxide solution. The layers were then extracted and separated with water three times, and the resultant organic layer was then washed with brine, dried with sodium sulfate and concentrated *in vacuo*. The crude mixture was further purified by column chromatography (4:1 hexanes:ethyl acetate) to yield a pale yellow solid (784 mg, 9.5%). ^{1}H NMR (400 MHz, Acetone-d$_6$ $\delta$) 7.73 (m, 2H), 7.55 (m, 2H), 7.48 (m, 4H), 7.40 (m, 1H), 7.28 (d, $J$ = 1.2 Hz, 1H), 7.25 (m, 3H), 7.17 (d, $J$ = 1.2 Hz, 1H), 2.03 (m, 6H). Elemental Analysis: Anal. Cacld. for $C_{23}H_{20}N_2$: C, 85.15 %; H, 6.21 %; N, 8.63 %. Found: C, 84.86 %; H, 6.28 %; N, 8.60 %

**1-(3,5-dimethyl-[1,1':4',1''-terphenyl]-4-yl)-2-phenyl-1H-imidazole (mipp-H).** A three neck flask was charged with 4-bromo-2,6-dimethylaniline (25.0 g, 125 mmol), glyoxal (18.1 g, 125 mmol) and 230 mL of methanol. The reaction mixture stirred at room temperature for 20 hours, upon which benzaldehyde (13.3 g, 125 mmol) and ammonium chloride (6.68 g, 125 mmol). A condenser was attached and the reaction was heated to reflux. Phosphoric acid (1.22 g, 12.5 mmol) was added after one hour and the reaction was left to reflux for an additional 24 hrs. The reaction was cooled to ambient temperature and concentrated *in vacuo* to remove the methanol solvent. The crude mixture was diluted with ethyl acetate and treated with 1 M aqueous sodium hydroxide solution. The layers were then extracted and separated with water three times, and the resultant organic layer was then washed with brine, dried with sodium sulfate and concentrated *in vacuo*. The crude mixture was further purified by column chromatography (4:1 hexanes:ethyl acetate) to yield 1-(4-

bromo-2,6-dimethylphenyl)-2-phenyl-$1\lambda^4,3\lambda^2$ -imidazole (2.5 g, 6%).. Then, one neck flask was charged with 1-(4-bromo-2,6-dimethylphenyl)-2-phenyl-$1\lambda^4,3\lambda^2$ -imidazole (2.50 g, 7.64 mmol), [1,1'-biphenyl]-4-ylboronic acid (3.03 g, 15.3 mmol), potassium carbonate (10.6 g, 76.4 mmol) and Tetrakis(triphenylphosphine)-palladium(0) (883 mg, 764 μmol). The flask was degassed and 75 ml of toluene and water (2:1) mixed solutions was added. The reaction was heated to reflux for 24 hours and was cooled to ambient temperature. The crude mixture was diluted with ethyl acetate and extracted with water three times, and the resultant organic layer was then washed with brine, dried with sodium sulfate and concentrated *in vacuo*. The crude mixture was further purified by column chromatography (4:1 hexanes:ethyl acetate) to yield a pale yellow solid (1.1 g, 36 %). $^1$H NMR (400 MHz, Acetone-d6) $\delta$ 7.88 – 7.83 (m, 2H), 7.82 – 7.78 (m, 2H), 7.76 – 7.72 (m, 2H), 7.62 (p, $J$ = 0.6 Hz, 2H), 7.53 – 7.45 (m, 4H), 7.42 – 7.36 (m, 1H), 7.29 (d, $J$ = 1.2 Hz, 1H), 7.27 – 7.23 (m, 3H), 7.19 (d, $J$ = 1.2 Hz, 1H), 2.05 (s, 6H). Elemental Analysis: Anal. Cacld. for $C_{29}H_{24}N_2$: C, 86.97 %; H, 6.04 %; N, 6.99 %. Found: C, 86.18 %; H, 5.97 %; N, 6.79 %

**Ir(mi)$_3$.** A pressure flask was charged with [(mi)$_2$IrCl]$_2$ dimer (80 mg, 0.053 mmol), mi-H ligand (70.1 mg, 0.267 mmol) and 7 mL of 50:50 dioxane water. The flask was degassed, sealed and heated to 130 $^o$C for six days. The reaction was then cooled to ambient temperature and filtered, washing the precipitate with water and cold methanol to give a pale yellow emissive solid (43.2 mg, 83 %). $^1$H NMR (400 MHz, Acetone-d$_6$ $\delta$) 7.11 (d, $J$ = 7.7 Hz, 2H), 6.99 (d, $J$ = 1.5 Hz, 1H), 6.84 (ddd, $J$ = 7.6, 1.3, 0.6 Hz, 1H), 6.76 (d, $J$ = 1.5 Hz, 1H), 6.49 (ddd, $J$ = 7.6, 7.2, 1.4 Hz, 1H), 6.35 (ddd, J = 7.7, 7.2, 1.4 Hz, 1H), 6.21 (ddd, $J$ = 7.8, 1.4, 0.6 Hz, 1H), 2.38 (s, 3H), 2.06 (s, 3H), 1.82 (s, 3H).

**Ir(miF)$_3$.** A pressure flask was charged with [(miF)$_2$IrCl]$_2$ dimer (330 mg, 0.186 mmol), miF-H ligand (418 mg, 1.27 mmol) and 23 mL of 50:50 dioxane water. The flask was degassed, sealed and heated to 130 °C for six days. The reaction was then cooled to ambient temperature, diluted in ethyl acetate and extracted with water three times. The organic layers were washed with brine, dried with sodium sulfate and concentrated *in vacuo*. The crude mixture was further purified by column chromatography (4:1 hexanes:ethyl acetate) to yield a bright yellow solid.(65.9 mg, 30 %). $^1$H NMR (400 MHz, Acetone-d6) $\delta$ 7.21 – 7.15 (m, 3H), 6.97 (d, $J$ = 1.9 Hz, 1H), 6.88 (d, $J$ = 1.9 Hz, 1H), 6.77 – 6.71 (m, 1H), 6.35 (d, $J$ = 8.1 Hz, 1H), 2.41 (s, 3H), 2.13 (s, 3H), 2.09 (s, 3H). Elemental Analysis: Anal. Cacld. for $C_{57}H_{48}F_9IrN_6$: C, 58.01 %; H, 4.10 %; N, 7.12 %. Found: C, 57.64 %; H, 3.94 %; N, 7.28 %

**Ir(mip)₃.** A round bottom was charged with iridium (III) acetylacetonate (175 mg, 0.357 mmol), mip-H ligand (580 mg, 1.79 mmol), and tridecane (135 mg, 0.357 mmol). A condenser was attached and the reaction was degassed, heated to 240 °C for 48 hours. The reaction was cooled to ambient temperature and column chromatography on the crude mixture was further purified by column chromatography (4:1 hexanes:ethyl acetate) to give a pale yellow emissive solid (104 mg, 25%). $^1$H NMR (400 MHz, Acetone-d$_6$ $\delta$) $\delta$ 7.79 (m, 2H), 7.65 (m, 2H), 7.52 (m, 2H), 7.43 (m, 1H), 7.13 (d, $J$ = 1.5 Hz, 1H), 6.90 (d, $J$ = 7.0 Hz, 1H), 6.87 (d, $J$ = 1.5 Hz, 1H), 6.54 (ddd, $J$ = 8.4, 7.3, 1.5 Hz, 1H), 6.40 (ddd, $J$ = 8.4, 7.1, 1.3 Hz, 1H), 6.34 (dd, $J$ =7.3, 1.5 Hz, 1H), 2.24 (s, 3H), 1.98 (s, 3H). Elemental Analysis: Anal. Cacld. for C$_{69}$H$_{57}$IrN$_6$: C, 71.29 %; H, 4.94 %; N, 7.23 %. Found: C, 70.59 %; H, 4.98 %; N, 6.97 %

**Ir(mipp)₃.** A round bottom was charged with iridium (III) acetylacetonate (175 mg, 0.357 mmol), mipp-H ligand (580 mg, 1.79 mmol), and tridecane (135 mg, 0.357 mmol). A condenser was attached and the reaction was degassed, heated to 240 $^{\circ}$C for 48 hours. The reaction was cooled to ambient temperature and column chromatography on the crude mixture was further purified by column chromatography (4:1 hexanes:ethyl acetate) to yield a pale yellow solid.to give a pale yellow emissive solid (104 mg, 25%).$^1$H NMR (400 MHz, Acetone-d6) $\delta$ 7.92 (d, $J$ = 7.6, 2H), 7.86 – 7.80 (d, $J$ = 7.6, 2H), 7.78 – 7.69 (m, 4H), 7.54 – 7.47 (t, 2H), 7.40 (t, $J$ = 9.1, 6.8, 2.2, 1.1 Hz, 1H), 7.16 (d, $J$ = 1.8, 0.9 Hz, 1H), 6.95 – 6.87 (m, 2H), 6.59 – 6.52 (t, 1H), 6.42 (t, $J$ = 7.1, 1.1 Hz, 1H), 6.38 – 6.33 (m, 1H), 2.26 (s, 3H), 2.00 (s, 3H). Elemental Analysis: Anal. Cacld. for C$_{87}$H$_{69}$IrN$_6$: C, 75.14 %; H, 5.00 %; N, 6.04 %. Found: C, 74.30 %; H, 5.00 %; N, 6.07 %

**NMR Measurements.**

$^1$H NMR spectra were recorded on a Varian 400 NMR spectrometer. Chemical shift data for each signal are reported in ppm and measured in deuterated acetone ((CD$_3$)$_2$CO).
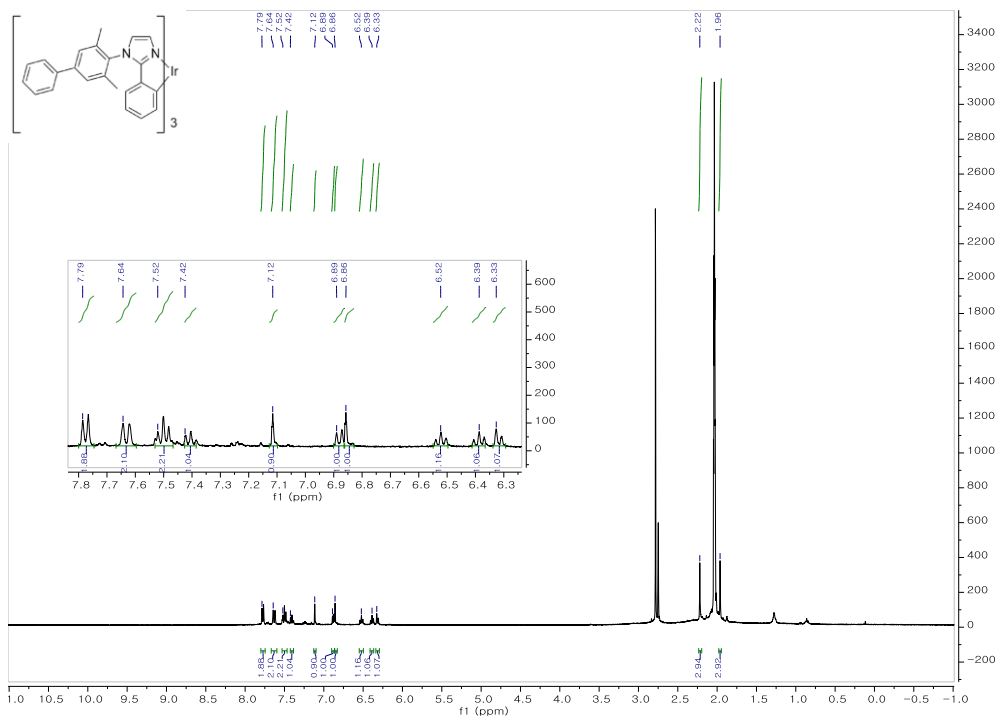
**Figure S1**. $^1$H NMR spectrum of Ir(mip)$_3$ in Acetone-d$_6$
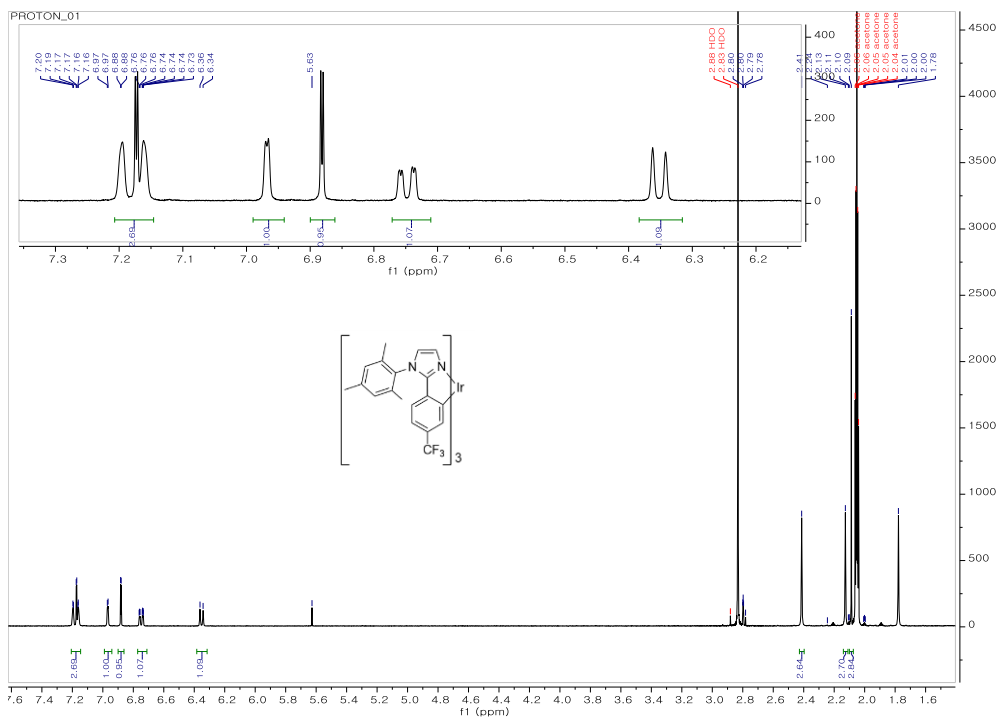


**Figure S2**. $^1$H NMR spectrum of Ir(miF)$_3$ in Acetone-d$_6$
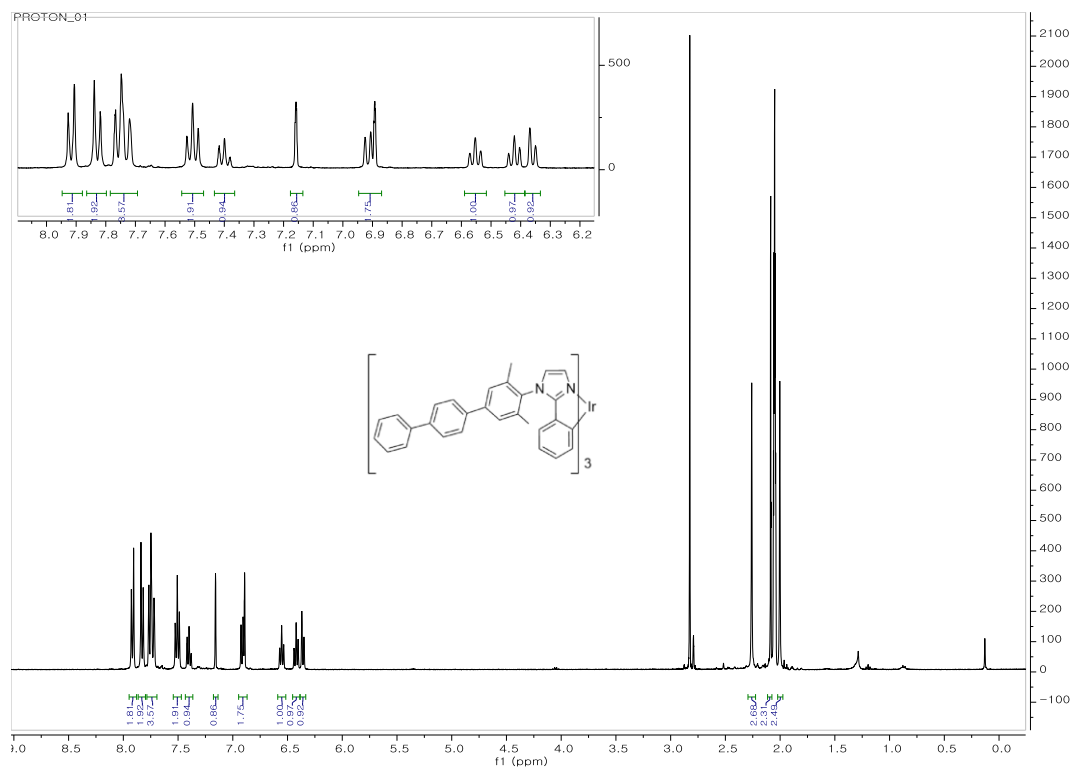
**Figure S3**. $^1$H NMR spectrum of Ir(mipp)$_3$ in Acetone-d$_6$
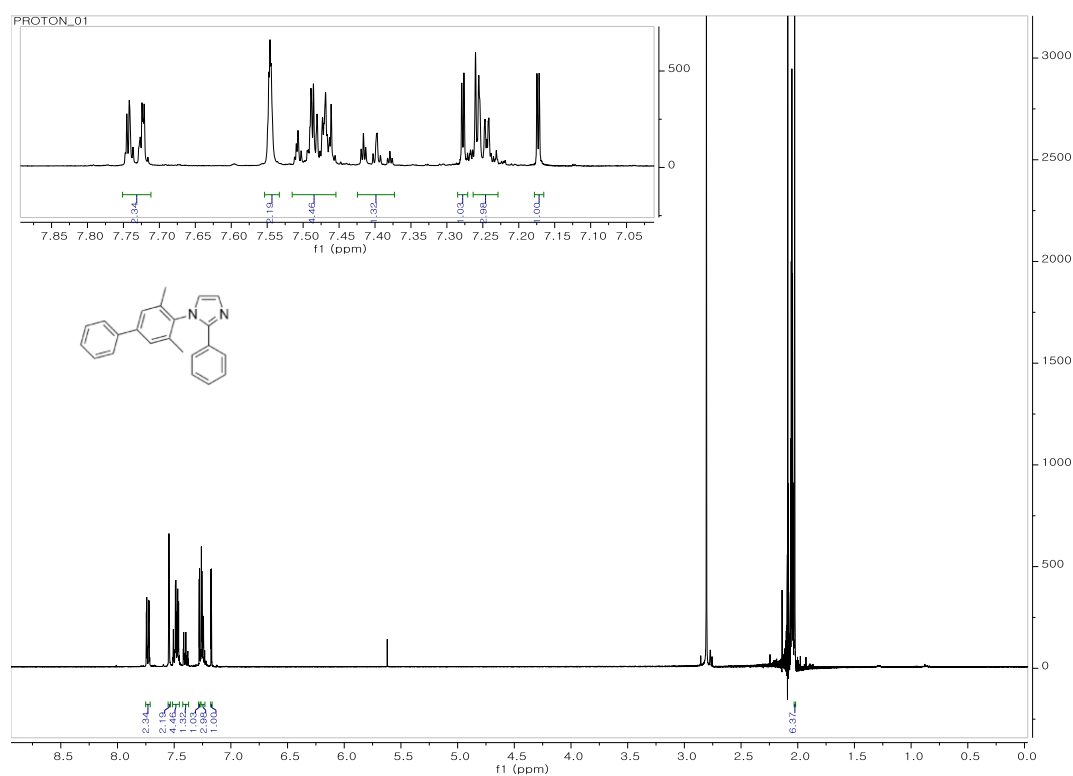


**Figure S4**. $^1$H NMR spectrum of mip-H in Acetone-d$_6$

**Figure S5**. ^{1}H NMR spectrum of miF-H in Acetone-d[6]



**Figure S6**. ^{1}H NMR spectrum of mipp-H in Acetone-d[6]
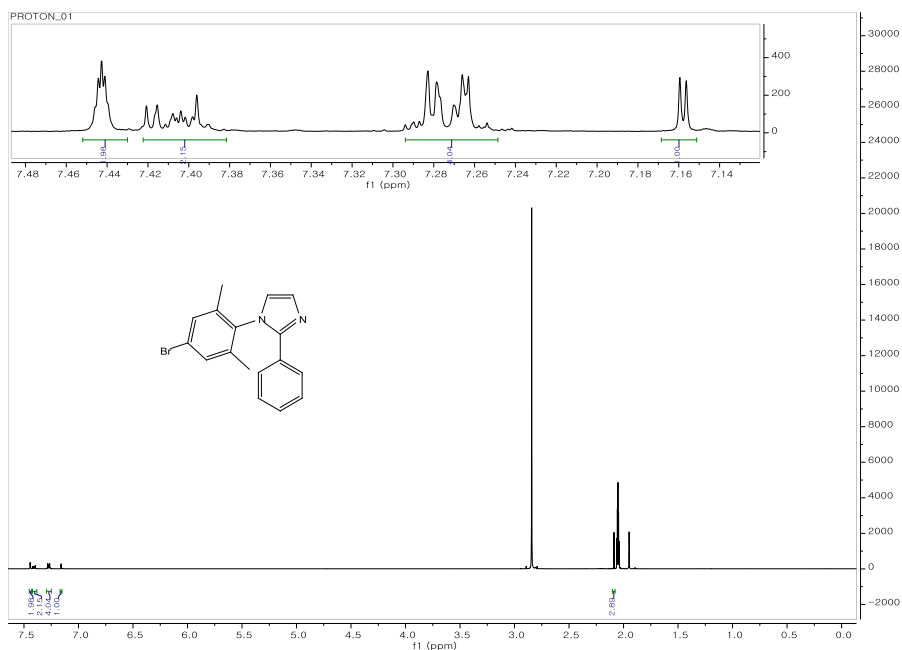
**Figure S7**. ^{1}H NMR spectrum of 1-(4-bromo-2,6-dimethylphenyl)-2-phenyl-1$\lambda^4$,3$\lambda^2$ -imidazole in Acetone-d$_6$

^{1}H NMR (400 MHz, Acetone-d6) $\delta$ 7.44 (m, 2H), 7.42 − 7.39 (m, 2H), 7.30 − 7.25 (m, 4H), 7.16 (d, $J$ = 1.3 Hz, 1H), 2.09 (s, 6H).
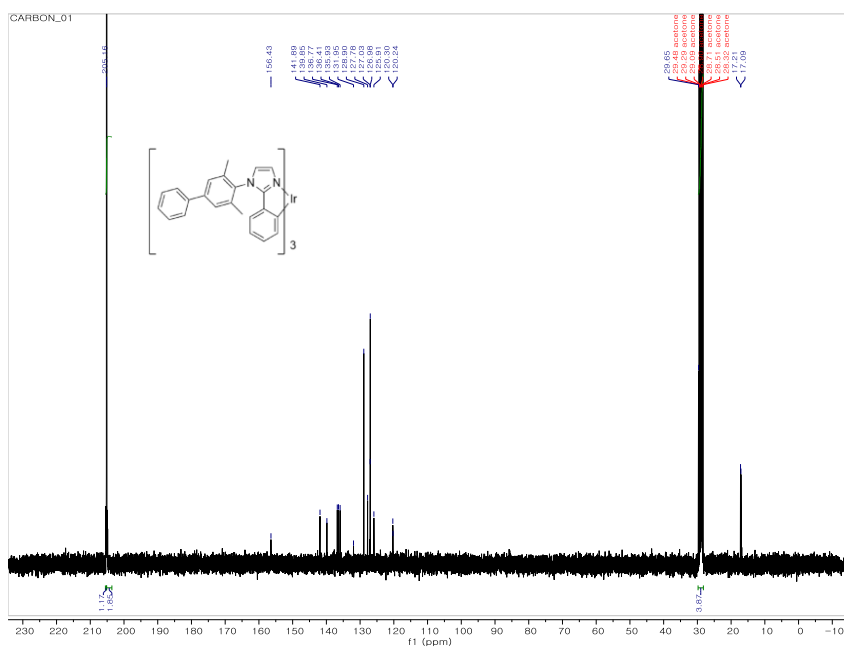


**Figure S8**. ^{13}C NMR spectrum of Ir(mip)$_3$ in Acetone-d$_6$

^{13}C NMR (101 MHz, acetone) $\delta$ 205.16, 156.43, 141.89, 139.85, 136.77, 136.41, 135.93, 131.95, 128.90, 127.78, 127.03, 126.98, 125.91, 120.30, 120.24, 17.21, 17.09.

12
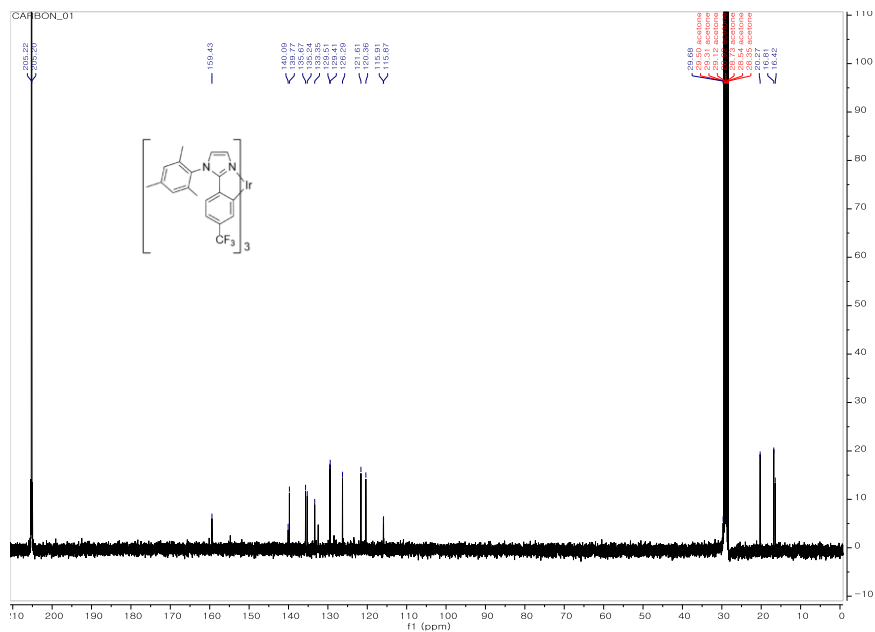
**Figure S9**. $^{13}$C NMR spectrum of Ir(miF)$_3$ in Acetone-d$_6$

$^{13}$C NMR (101 MHz, acetone) $\delta$ 159.43, 140.09, 139.77, 135.67, 135.24, 133.35, 129.51, 129.41, 126.29, 121.61, 120.36, 115.91, 115.87, 20.27, 16.81, 16.42.
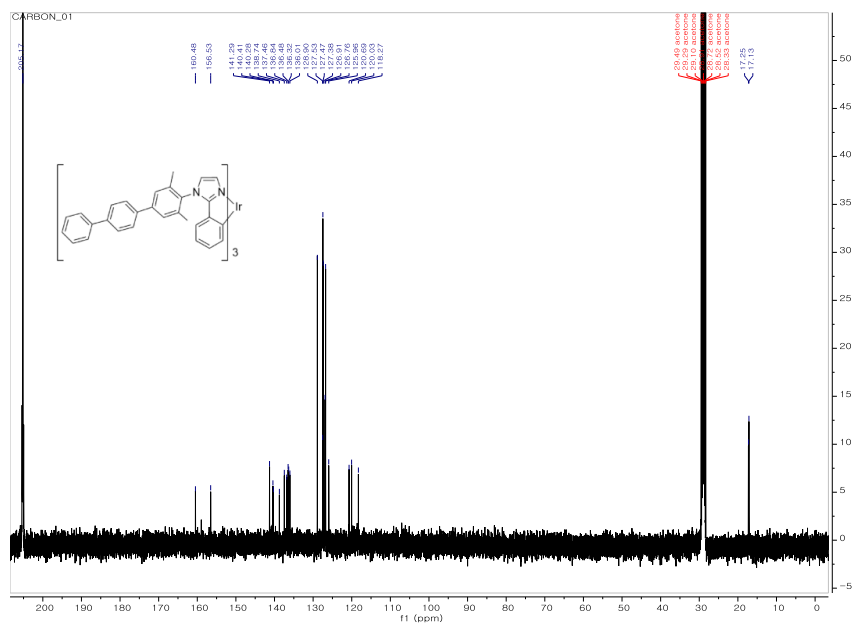


**Figure S10**. $^{13}$C NMR spectrum of Ir(mipp)$_3$ in Acetone-d$_6$

$^{13}$C NMR (101 MHz, acetone) $\delta$ 205.17, 160.48, 156.53, 141.29, 140.41, 140.28, 138.74, 137.46, 136.84, 136.48, 136.32, 136.01, 128.90, 127.53, 127.47, 127.38, 126.91, 126.76, 125.96, 120.69, 120.03, 118.27, 17.25, 17.13.
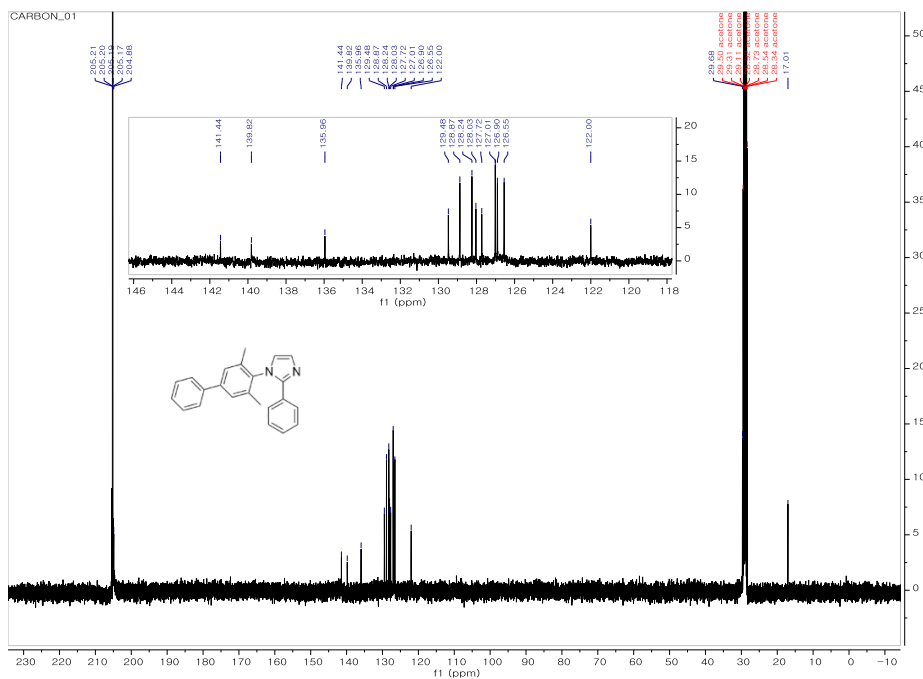
**Figure S11.** $^{13}C$ NMR spectrum of mip-H in Acetone-$d_6$

$^{13}C$ NMR (101 MHz, acetone) $\delta$ 141.44, 139.82, 135.96, 129.48, 128.87, 128.24, 128.03, 127.72, 127.01, 126.90, 126.55, 122.00, 17.01.
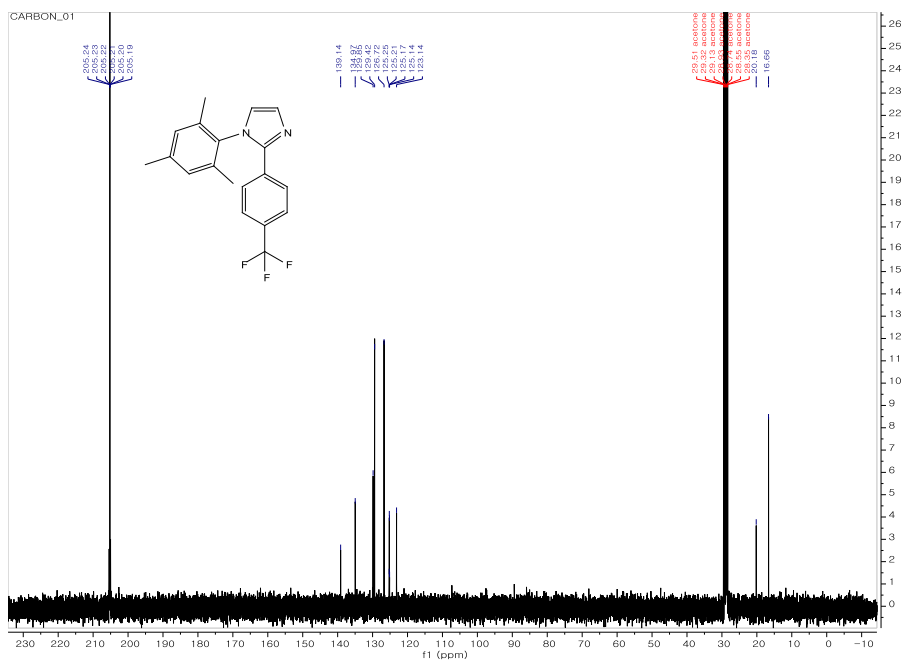


**Figure S12.** $^{13}C$ NMR spectrum of miF-H in Acetone-$d_6$

$^{13}C$ NMR (101 MHz, acetone) $\delta$ 139.14, 134.97, 129.85, 129.42, 126.72, 125.25, 125.21, 125.17, 125.14, 123.14, 20.18, 16.66.
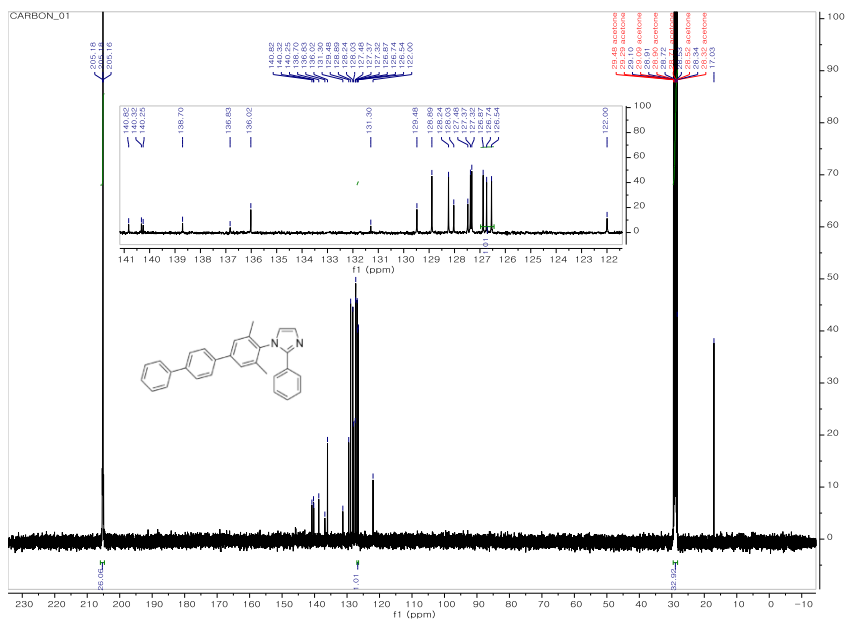
**Figure S13.** ^{13}C NMR spectrum of mipp-H in Acetone-d$_6$

^{13}C NMR (101 MHz, acetone) $\delta$ 205.18, 205.18, 205.16, 140.82, 140.32, 140.25, 138.70, 136.83, 136.02, 131.30, 129.48, 128.89, 128.24, 128.03, 127.48, 127.37, 127.32, 126.87, 126.74, 126.54, 122.00, 17.03.
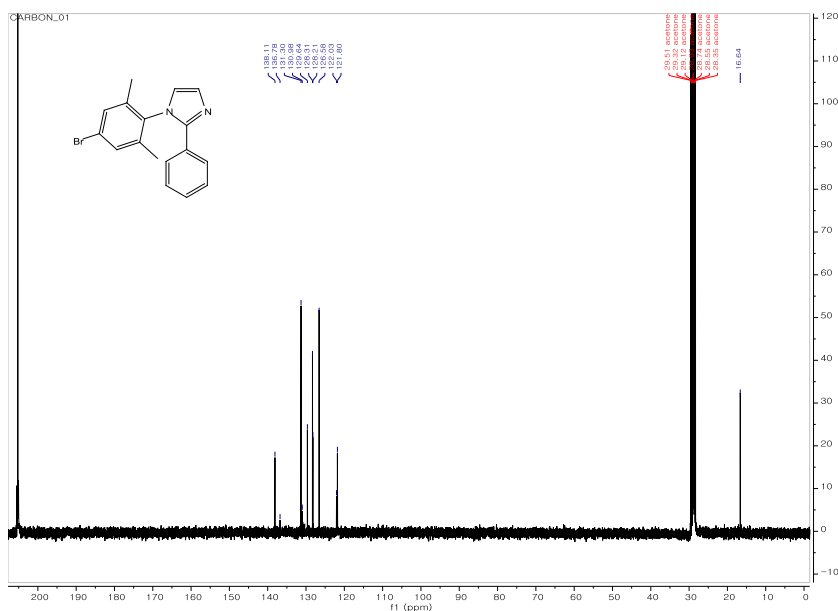


**Figure S14.** 13C NMR spectrum of 1-(4-bromo-2,6-dimethylphenyl)-2-phenyl-1$\lambda^4$,3$\lambda^2$-imidazole in Acetone-d6

^{13}C NMR (101 MHz, acetone) $\delta$ 138.11, 136.78, 131.30, 130.98, 129.64, 128.31, 128.21, 126.58, 122.03, 121.80, 16.64.

**Photophysical Measurements.**

Photoluminescence spectra were measured using a QuantaMaster Photon Technology International phosphorescence/fluorescence spectrofluorometer. Phosphorescent lifetimes were measured by time-correlated single-photon counting using an IBH Fluorocube instrument equipped with an LED excitation source. Quantum yield measurements were carried out using a Hamamatsu C9920 system equipped with a xenon lamp, calibrated integrating sphere and model C10027 photonic multi-channel analyzer (PMA). UV−vis spectra were recorded on a Hewlett-Packard 4853 diode array spectrometer. The samples were deaerated by extensive sparging with $N_2$.

| Table S1. Absorption data for the Ir complexes **1**–**3**. |
|---|
| $\lambda_{max}$(nm) ($\varepsilon$, $10^3$ $M^{-1}$ $cm^{-1}$) |
| Ir(mi)₃ (**1**)    304 (10.7), 350 (12.6), 380 (sh, 8.13), 413 (sh, 3.47), 459 (sh, 0.461) |
| Ir(miF)₃ (**2**)    353 (11.3), 386 (sh, 6.67), 428 (sh, 2.52), 473 (sh, 0.529) |
| Ir(mip)₃ (**3**)    340 (14.8), 380 (sh, 9.25), 415 (sh, 3.86), 459 (sh, 0.722) |



**Figure S15.** Absorption spectra of (1), (2) and (3) in 2-MeTHF
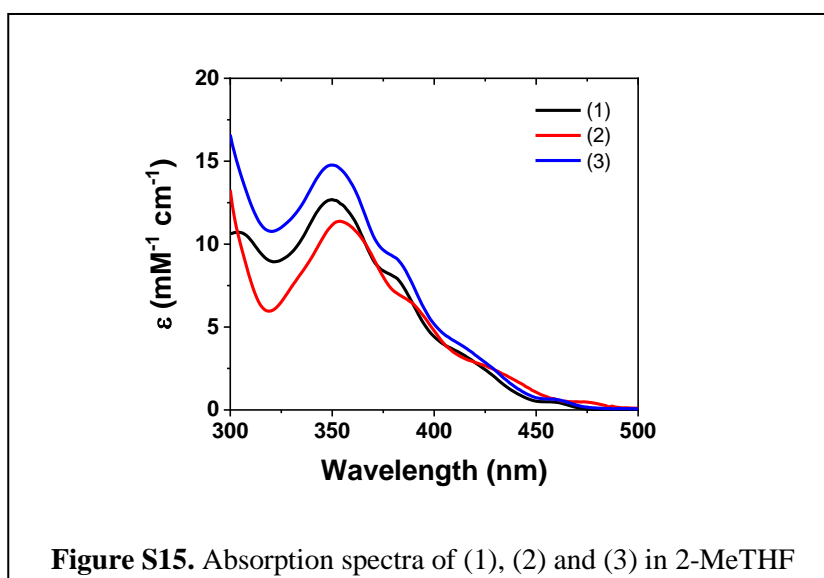
The absorption spectra of (1), (2), and (3) are shown in Figure S15 and data are summarized in Table S1. All of the three complexes show intense high energy bands ($\lambda < 360$

nm, $\varepsilon > 10$ mM$^{-1}$ cm$^{-1}$) corresponding to $\pi{\rightarrow}\pi^*$ transition on the cyclometalated ligands. Broad and less intense absorption bands at low energy ($\lambda = 360\text{-}440$ nm, $\varepsilon > 2$ x 10 mM$^{-1}$ cm$^{-1}$) are assigned to Metal-to Ligand Charge Transfer transitions (MLCT[1]). MLCT[3] transitions are apparent at lower energy ($\lambda > 450$ nm, $\varepsilon < 0.1$ mM$^{-1}$cm$^{-1}$) in the absorption spectra with weaker intensity due to limited spin-orbit coupling with the single states by the iridium metal center.



**Figure S16.** Absorption and emission spectrum of Ir(mipp)$_3$ in 2-MeTHF

**Table S2.** Photoluminescence (PL) data for the Ir(mi)$_3$, Ir(miF)$_3$, Ir(mip)$_3$ and Ir(mipp)$_3$.[a]

| | 298 K | | | | 77 K |
|---|---|---|---|---|---|
| | $\lambda_{max}$ (nm) [$\Phi$][b] | $\tau$ ($\mu$s)[c] | $k_r$ ($10^5$ s$^{-1}$)[d] | $k_{nr}$ ($10^4$ s$^{-1}$)[d] | $\lambda_{0-0}$ (nm) [$\tau$ ($\mu$s)][c] |
| **Ir(mi)$_3$** | 470 [0.91] | 2.0 | 4.5 | 5.0 | 464 [2.7] |
| **Ir(miF)$_3$** | 484 [0.99] | 2.5 | 4.0 | 0.4 | 484 [3.2] |
| **Ir(mip)$_3$** | 472 [0.98] | 1.8 | 5.4 | 1.6 | 466 [2.3] |
| **Ir(mipp)$_3$** | 470 [1.00] | 7.9 | 1.3 | < 0.013 | 468 [180 (85%)/2100 (15%)] |

[a] In 2-MeTHF. [b] Photoluminescent quantum yield. [c] Error is ± 5%. [d] Derived using $\Phi = k_r\tau = k_r/(k_r + k_{nr})$.

**Electrochemical Properties**

The redox properties of the (1), (2), (3) and (4) were investigated by cyclic voltammetry and differential pulse voltammetry in acetonitrile solution with 0.1 M TBAF (Figure S17). Oxidation potentials of (1), (3) and (4) are 0.07 V, 0.10 V and 0.10 V, respectively with reversibility. These values are close to $E_{ox1} = 0.10$ V- 0.12 V which are reported with other *tris*-cyclometalated phenylimidazole iridium complexes. (2) is more difficult to oxidize ($E_{ox1} = 0.40$ V) compared to others due to stabilization of HOMO by the presence of electron withdrawing trifluoromethyl group on aryl moiety as shown in Table S4. Reduction potential of (1) could not be measured while (2) and (3) show reduced reduction wave ($E_{red1} = $ -2.84V, -2.86V respectively). Significant difference in reduction potentials between (1) and the rest can be explained by considering distribution of LUMO. As shown in Table S4, first reduction of (2) can be assigned to phenyl imidazole ligand. Therefore, trifluoromethyl moiety on aryl group stabilizes not only the HOMO but also the LUMO of (2), leading to a smaller reduction potential. On the other hand, LUMO of (1) and (3) are mainly located on mesityl and phenyl xylyl ligand respectively. The second phenyl group attached to mesityl imidazole ligand allows for the electrons to delocalize across extended xylyl phenyl backbone of the ligand, resulting in stabilization of the LUMO of (3).
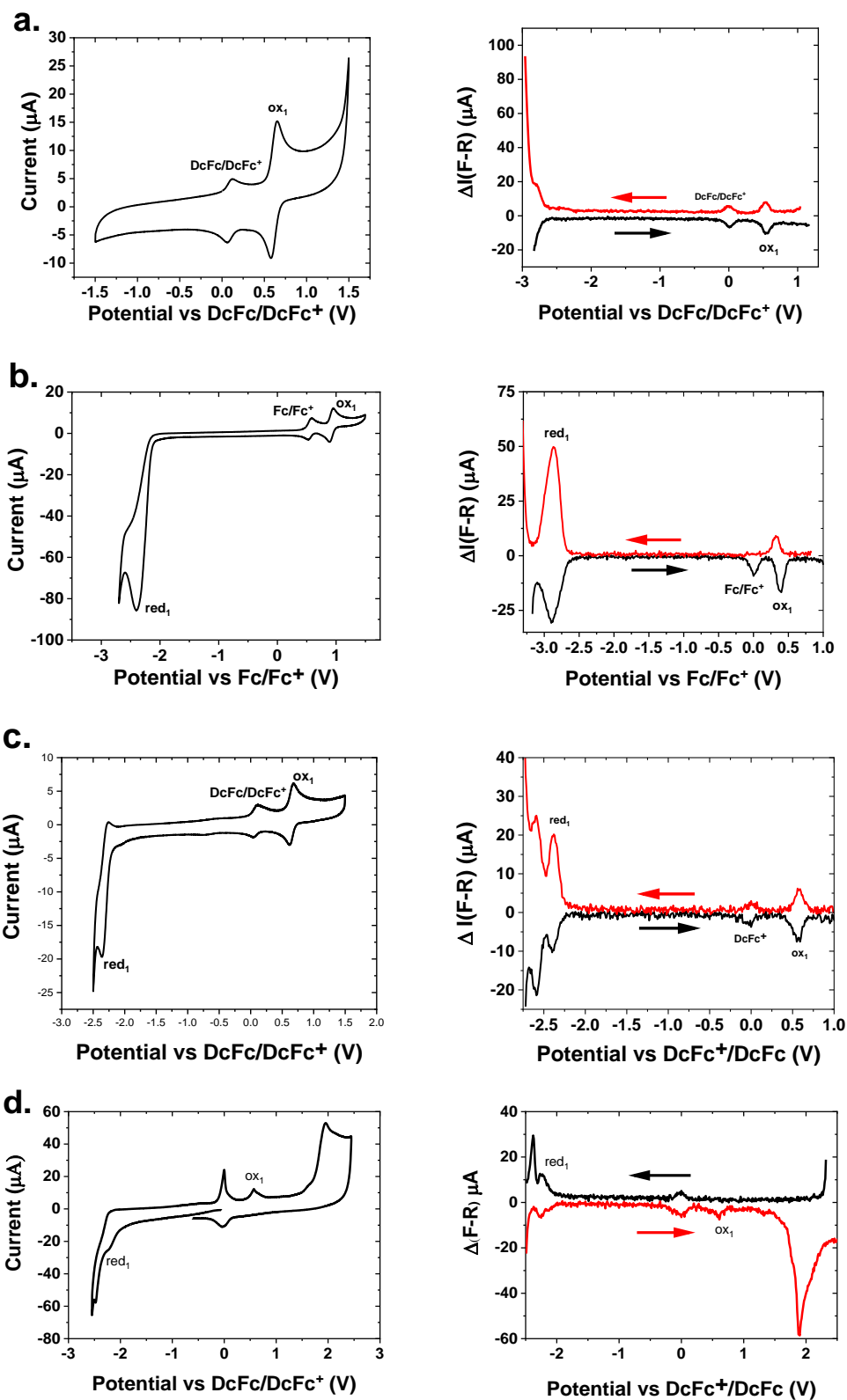
**Figure S17.** Cyclic Voltammetry (CV) and Differential Pulse Voltammetry (DPV) in MeCN of a.) $Ir(mi)_3$ in $DcFc/DcFc^+$, b.) $Ir(miF)_3$ in $Fc/Fc+$, c.) $Ir(mip)_3$ in $DcFc/DcFc^+$, d.) $Ir(mipp)_3$ in $DcFc/DcFc^+$. DPV of $Ir(mi)_3$ was measured in DMF.

**Molecular computational modeling**

Aspect Ratio Calculation

To compute the aspect ratios, the 3D moments matrix of each complex was computed by taking the Ir atom as the center. The moments matrix ($M$) is then computed as:

$$M = \begin{bmatrix} \sum_i (x_i - x_{Ir})^2 & \sum_i (x_i - x_{Ir})(y_i - y_{Ir}) & \sum_i (x_i - x_{Ir})(z_i - z_{Ir}) \\ \sum_i (x_i - x_{Ir})(y_i - y_{Ir}) & \sum_i (y_i - y_{Ir})^2 & \sum_i (y_i - y_{Ir})(z_i - z_{Ir}) \\ \sum_i (x_i - x_{Ir})(z_i - z_{Ir}) & \sum_i (y_i - y_{Ir})(z_i - z_{Ir}) & \sum_i (z_i - z_{Ir})^2 \end{bmatrix}$$

where, $x_i$, $y_i$, $z_i$ are the positional coordinates of an atom i in the molecule and $x_{Ir}$, $y_{Ir}$, $z_{Ir}$ are the coordinates of the central Ir atom. The matrix $M$ is then diagonalized to obtain the corresponding eigenvalues, $\lambda_1$, $\lambda_2$ and $\lambda_3$. Then, $\sqrt{\lambda_1}$, $\sqrt{\lambda_2}$ and $\sqrt{\lambda_3}$ represent the relative length of the principal semi-axes of a hypothetical ellipsoid hull that represents the molecule (i.e. $a \propto \sqrt{\lambda_1}$, $b \propto \sqrt{\lambda_2}$, $c \propto \sqrt{\lambda_3}$).

In our case, since we are dealing with homoleptic octahedral complexes, the lengths of at least two of the semi-axes are expected to be similar ($a \approx b$). The aspect ratio can then be computed as the ratio between $a$ and $c$. The DFT ground state optimized geometries were used to compute the aspect ratios in all cases.

**Table S3.** Calculated aspect ratio of all compounds studied in the paper

| | Ir(ppy)$_3$ | Ir(ppyCF)$_3$ | Ir(mi)$_3$ | Ir(miF)$_3$ | Ir(mip)$_3$ | D1[*] | D2[*] | D3[*] | D4[*] | D5[*] |
|---|---|---|---|---|---|---|---|---|---|---|
| Aspect ratio | 1.2 | 1.0 | 2.2 | 1.9 | 3.0 | 1.3 | 1.9 | 2.1 | 2.7 | 2.9 |

[*]Molecules in reference[3]

Energy and permanent dipole moment calculations

The ground (S$_0$) and triplet (T$_1$) state geometries of the complexes reported here were optimized at the B3LYP/LACV3P** level using the Jaguar (v. 9.4 release 15) program

within the Material Science suite[4] developed by Schrödinger, LLC. To compute the TDMs

for phosphorescent ($T_1 \rightarrow S_0$) emission in these molecules, time-dependent density functional

theory (TDDFT) with the zero order regular approximation (ZORA) approach[5] (SOC-

TDDFT) as implemented in Jaguar was utilized. The ZORA Hamiltonian incorporates spin-

orbit coupling (SOC) effects essential to compute TDMs associated with triplet ($T_1 \rightarrow S_0$)

emission. The SOC-TDDFT calculations were performed on structures optimized in the $T_1$

state using the B3LYP functional and a mixed basis set utilizing the DYALL-2ZCVP-ZORA-

J-Pt-Gen set for the Ir atom and the 6-31G** set for the remaining atoms.
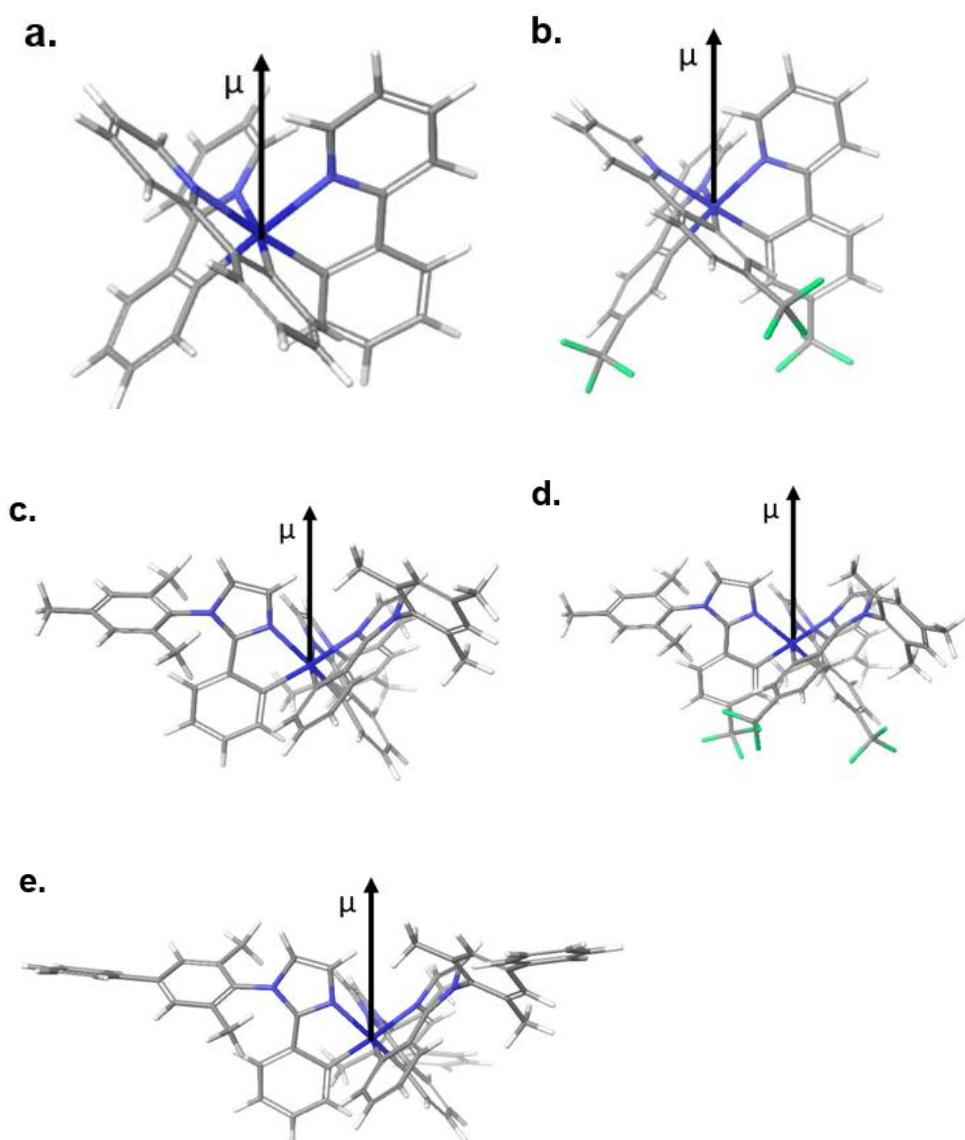
**Figure S18.** Orientation of permanent dipole moments of dopants relative to the molecular frame. Ir(ppy)$_3$ (a), Ir(ppy-CF$_3$)$_3$ (b), Ir(mi)$_3$ (c), Ir(miF)$_3$ (d) and Ir(mip)$_3$ (e). The length of the dipole does not represent its magnitude.



TCTA       mCBP       26DCzPPy       HT       ET
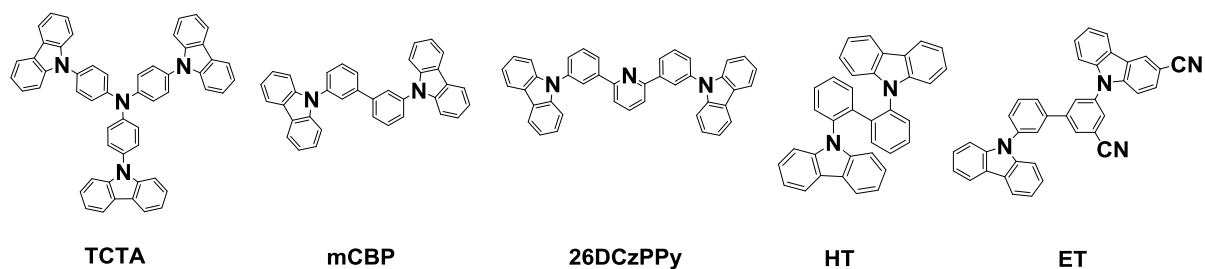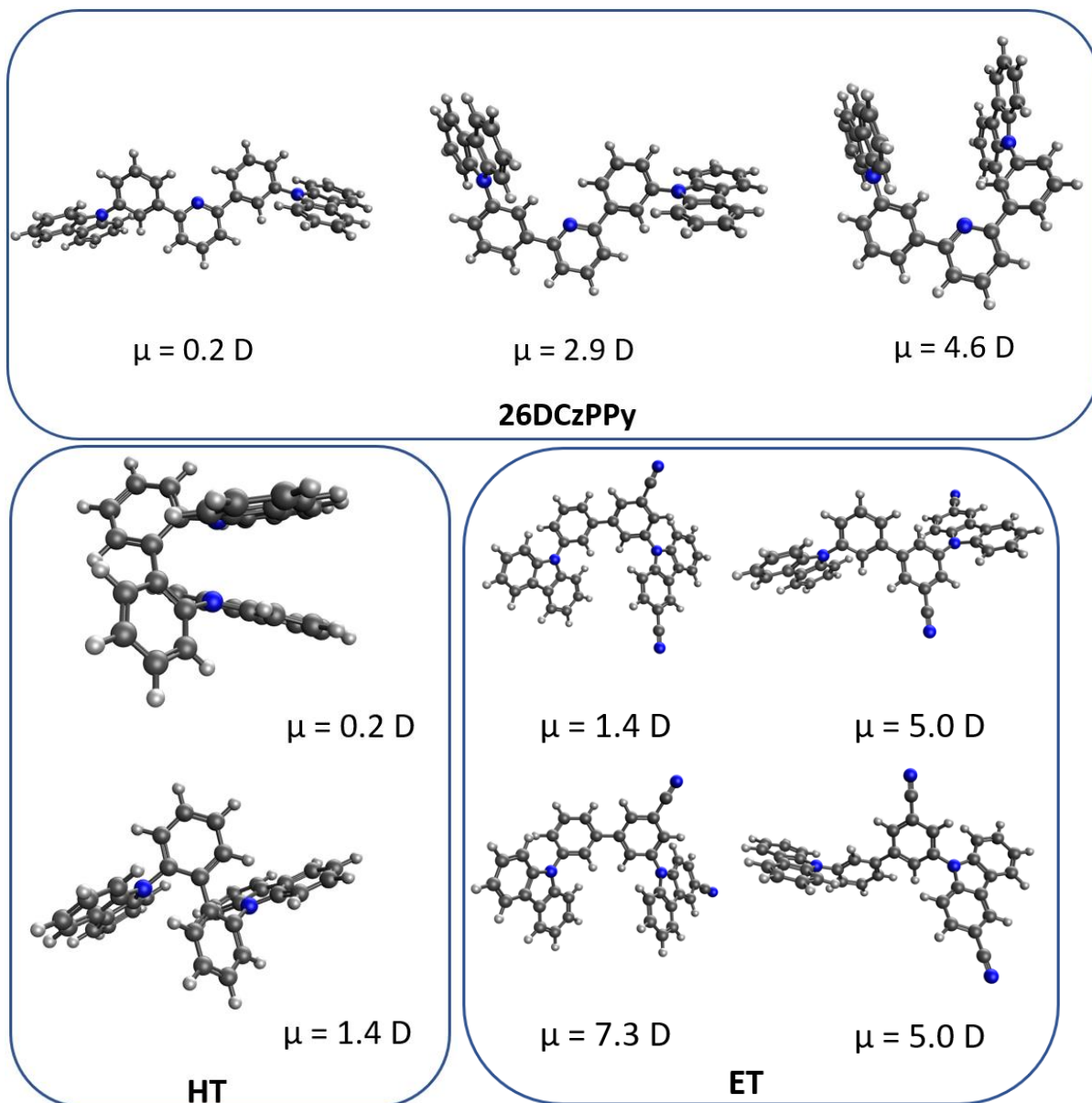
**Figure S19.** Molecular structures of host materials used in the paper and reference [6] along with the structures of different conformers

**Table S4.** Dipole moments of host materials obtained from DFT calculations.
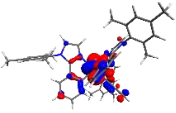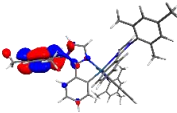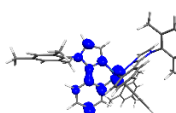
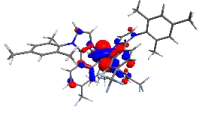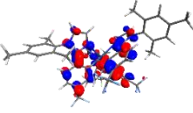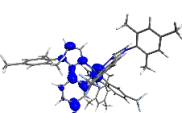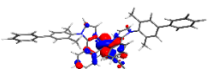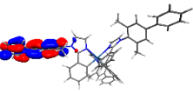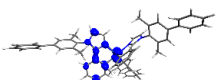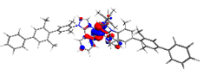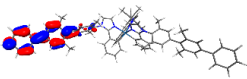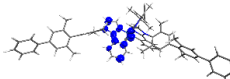| Compound | Dipole moment ($S_0$ in Debye) |
|---|---|
| TCTA | 0.1 |
| mCBP [a] | 0.8 |
| 26DCzPPY | 2.6 [c] |
| HT [b] | 0.8 [c] |
| ET [b] | 4.7 [c] |

a) Crystal structure of mCBP from reference [7] is used b) Host materials from reference [6]   c) The value listed is the average of dipole moments

found for the different conformers of the molecule shown above.

**Table S5.** HOMO, LUMO and triplet density distribution of all complexes

| | HOMO | LUMO | Triplet density |
|---|---|---|---|
| **Ir(mi)$_3$** | | | |
| **Ir(miF)$_3$** | | | |
| **Ir(mip)$_3$** | | | |
| **Ir(mipp)$_3$** | | | |

**Transition dipole moment vector (TDM) alignment measurements**

All thin films used in PL measurements were deposited at 0.9 Å/s and 0.1 Å/s for the host and dopant molecules, respectively, on 0.2 mm thick fused silica glass by vacuum thermal evaporation in a chamber with a base pressure of $1 \times 10^{-7}$ torr. The deposition rate and thicknesses were controlled using a quartz crystal thickness monitor. Following the deposition, devices were encapsulated using an epoxy seal around the edge of a 1.57 mm thick cover glass in an ultrapure $N_2$ environment.

Angle dependent *p*-polarized emission spectroscopy (ADPS) [8] was used to determine the ordering of Ir(mi)$_3$, Ir(mip)$_3$ and Ir(miF)$_3$ in doped thin films. The substrate was placed perpendicular to the plane of detection and the emission is outcoupled from the substrate

using a 2 cm radius, half-cylindrical lens. The emission along the plane of detection was decomposed into transverse electric (*TE*) and magnetic (*TM*) modes using a polarization analyzer. A motorized stage was used to position the detector. Simulations of the angular intensity profile are based on the dyadic Green's function in a birefringent medium.[9] A least-squares algorithm was used to fit the experimental data to the simulation. The refractive indices and extinction coefficients of materials were measured using variable-angle spectroscopic ellipsometry.

Fourier-plane imaging microscopy (FPIM) was used to determine the orientation of $Ir(ppy)_3$ and $Ir(ppyCF_3)_3$ in doped films.[10] The Fourier microscope consists of two parts, (i) an inverted fluorescence microscope (Olympus IX73) with a 325 nm He-Cd continuous-wave laser, and (ii) a system comprising Fourier lens (Thorlabs), optical filters, a linear polarizer, and a spectrometer with a $1024\times1024$ charge coupled device (CCD) array (Princeton Instruments). The photoluminescence of the sample was coupled through an oil immersion objective ($\times100$, NA=1.40, Olympus). The Fourier lens ($f = 300$ mm) was used to reconstruct the Fourier image plane on the CCD. A long-pass filter was used to prevent the laser beam being incident on the CCD, while a band-pass filter with the pass band near the peak wavelength of the dopant photoluminescence was also placed in the optical path. A linear polarizer separates the emission into two the orthogonal planes corresponding to the *p*- and *s*-polarized plane modes. The obtained emission contour was fitted according to the reported method.[10] To suppress imaging artefacts in the high-*k* region, the *k*-space fitting was performed over a limited range of $-1.1 < k_x/k_0 < 1.1$.[11]
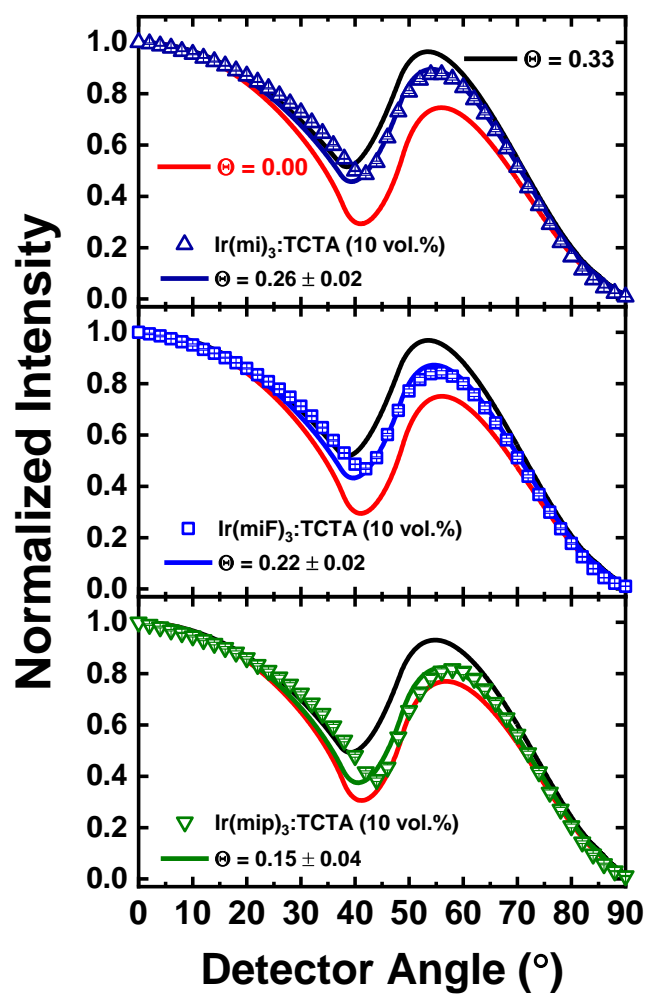
**Figure S20.** ADPS measurements and simulations for films of TCTA doped with Ir(mi)$_3$ (Top), Ir (miF)$_3$ (Middle) and Ir(mip)$_3$ (Bottom) at 10 vol% doping ratio. The measured data have been fitted black (Isotropic) and red (Perfectly horizontal) lines to determine the degree of orientation. Ir(mi)3 $\Theta$ = 0.26; Ir(miF)3 $\Theta$ = 0.22; and Ir(mip)3 $\Theta$ = 0.15 in TCTA respectively.
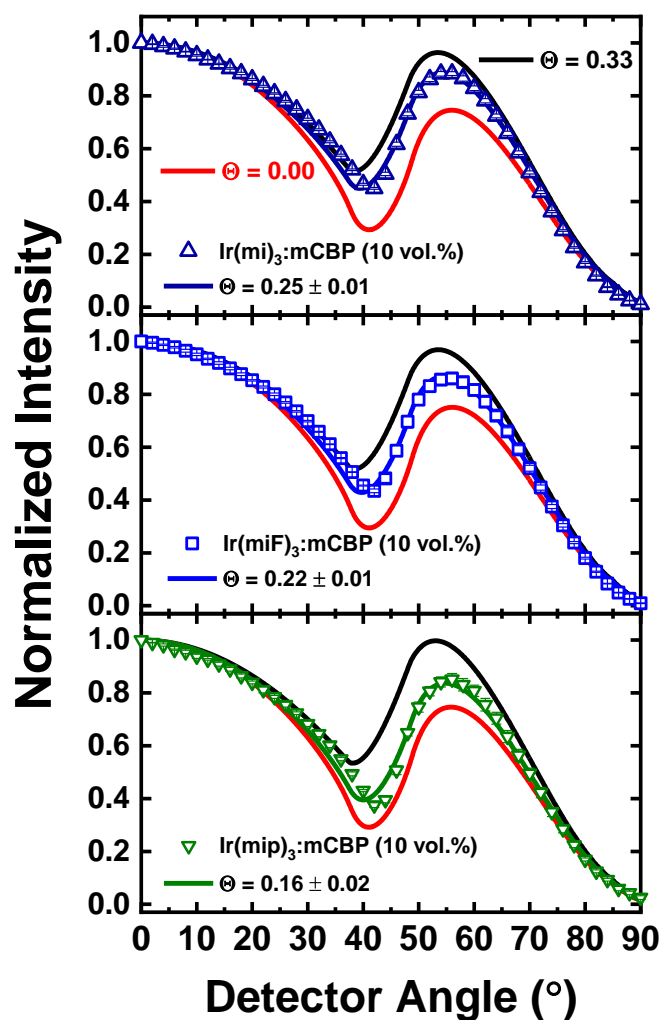
**Figure S21.** ADPS measurements and simulations for films of mCBP doped with Ir(mi)$_3$ (Top), Ir (miF)$_3$ (Middle) and Ir(mip)$_3$ (Bottom) at 10 vol% doping ratio. The measured data have been fitted (black and red lines) to determine the degree of orientation. Ir(mi)$_3$ $\Theta$ = 0.25; Ir(miF)$_3$ $\Theta$ = 0.22; and Ir(mip)$_3$ $\Theta$ = 0.16 in mCBP respectively.

**Figure S22**. FPIM intensity profiles in the p-polarized dipole plane (pPP) and s-polarized dipole p lane (sPP) for films of TCTA:26DCzPPy 2:1 doped with Ir(ppyCF$_3$)$_3$ (a) and Ir(ppy)$_3$ (b) at 10 vo l% doping ratio to determine the degree of orientation. Experimental data and simulated fits are expressed as points, solid lines respectively. Insets are the molecular structure of Ir(ppyCF$_3$)$_3$ and Ir(ppy)$_3$ respectively. $\Theta$ = 0.29 for Ir(ppyCF$_3$)$_3$ and $\Theta$ = 0.35 for Ir(ppy)$_3$ in TCTA:26DCzPPy 2:1 mixed host respectively.

**OLED Studies and Device Simulation**

<u>OLED fabrication</u>

All thin films used in PL measurements were deposited at 0.9 Å/s and 0.1 Å/s for the host and

dopant molecules, respectively, on 0.2 mm thick fused silica glass by vacuum thermal

evaporation in a chamber with a base pressure of $1 \times 10^{-7}$ torr. The deposition rate and

thicknesses were controlled using a quartz crystal thickness monitor. Following the deposition, devices were encapsulated using an epoxy seal around the edge of a 1.57 mm thick cover glass in an ultrapure $N_2$ environment. PhOLEDs were grown by vacuum thermal evaporation (VTE) on pre-cleaned glass substrates coated with 70 nm thick indium tin oxide (ITO). The device structures were: 70 nm ITO/50 nm 4,4′-cyclohexylidenebis(N,N-bis(4-methylphenyl)benzenamine) (TAPC) /EML, 15 nm Co-host, *tris*(4-carbazoyl-9-yl-phenyl)amine (TCTA): 2,6-bis(3-(9H-carbazol-9-yl)phenyl)pyridine (26DCzPPy) 2 mixed with the dopants doped at 10 vol.%/50 nm 3,3',5,5'-tetra[(*m*-pyridyl)-phen-3-yl]biphenyl (BP4mPy)/1.5 nm Li quinolate/Al. The current density-voltage (*J-V*) characteristics were measured using a parameter analyzer (HP4145, Hewlett-Packard) and a calibrated photodiode (FDS1010-CAL, Thorlabs, Inc.) following standard procedures.[12] The emission spectra at *J* = 100 mA cm$^{-2}$ were measured using a calibrated spectrometer (USB4000, Ocean Optics, Inc) connected to the device via an optical fiber (P400-5-UV-VIS, Ocean Optics, Inc).

Device simulation

The modal power distribution of the PHOLED was calculated based on Green's function analysis.[9, 13] The device structure used for the simulation is: ITO 70 nm / 1,1-bis[(di-4-tolylamino)phenyl]cyclohexane (TAPC) 50 nm / *tris*(4-carbazoyl-9-ylphenyl)amine (TCTA) : 2,6-bis(3-(carbazol-9-yl)phenyl)pyridine (26DCzPPy) 2 mixed host 15 nm (Active Layer) / (BP4mPy) 3,3',5,5'-tetra[(*m*-pyridyl)-phen-3-yl]biphenyl 50 nm / Al 100 nm. Refractive indices for all materials were measured using the variable-angle spectroscopic ellipsometry at $\lambda$ = 470 nm, 484 nm, 472 nm, 530 nm corresponding to the peak wavelength for Ir(mi)$_3$, Ir(miF)$_3$, Ir(mip)$_3$, Ir(ppy)$_3$ and Ir(ppyCF$_3$)$_3$ respectively. The dipole orientation of each dopant ($\Theta$ = 0.26, 0.22, 0.15, 0.35, 0.29 for Ir(mi)$_3$, Ir(miF)$_3$, Ir(mip)$_3$, Ir(ppy)$_3$, Ir(ppyCF$_3$)$_3$ respectively) measured via angle dependent p-polarized emission spectrum and Fourier-plane

imaging microscopy was used in the simulations[14] and the emitter location was assumed to be in the cathode (Al) side of the EML. The radiative efficiencies of each Ir(miX)$_3$ doped into the TCTA : 26DCzPPy 2 mixed host matrix were measured with an integrating sphere following the previously reported method.[15]

## References

[1]     M. Nonoyama, *Bulletin of the Chemical Society of Japan* **1974**, *47*, 767.

[2]     a) A. B. Tamayo, B. D. Alleyne, P. I. Djurovich, S. Lamansky, I. Tsyba, N. N. Ho, R. Bau, M. E. Thompson, *Journal of the American Chemical Society* **2003**, *125*, 7377; b) A. Singh, K. Teegardin, M. Kelly, K. S. Prasad, S. Krishnan, J. D. Weaver, *J. Organomet. Chem.* **2015**, *776*, 51; c) K. Udagawa, H. Sasabe, C. Cai, J. Kido, *Adv. Mater.* **2014**, *26*, 5062; d) J. Y. Zhuang, W. F. Li, W. C. Wu, M. S. Song, W. M. Su, M. Zhou, Z. Cui, *New J. Chem.* **2015**, *39*, 246.

[3]     J. S. Kim, D. Jeong, H. J. Bae, Y. Jung, S. Nam, J. W. Kim, S.-G. Ihn, J. Kim, W.-J. Son, H. Choi, S. Kim, *Adv. Opt. Mater.* **2020**, *8*, 2001103.

[4]     S. Materials Science Suite 2016-4, LLC, New York, NY, 2016.

[5]     a) E. van Lenthe, E. J. Baerends, J. G. Snijders, *J.Chem.Phys.* **1994**, *101*, 9783; b) E. vanLenthe, J. G. Snijders, E. J. Baerends, *J. Chem. Phys.* **1996**, *105*, 6505; c) E. v. Lenthe, E. J. Baerends, J. G. Snijders, *J.Chem.Phys.* **1993**, *99*, 4597.

[6]     J. S. Kim, D. Jeong, H. J. Bae, Y. Jung, S. Nam, J. W. Kim, S. G. Ihn, J. Kim, W. J. Son, H. Choi, S. Kim, *Advanced Optical Materials* **2020**, *8*.

[7]     J.-X. Wang, Y.-G. Fang, C.-X. Li, L.-Y. Niu, W.-H. Fang, G. Cui, Q.-Z. Yang, *Angew. Chem. Int. Ed.* **2020**, *59*, 10032.

[8]     a) J. Frischeisen, D. Yokoyama, C. Adachi, W. Brutting, *Appl. Phys. Lett.* **2010**, *96*; b) C. K. Moon, S. Y. Kim, J. H. Lee, J. J. Kim, *Opt. Express* **2015**, *23*, A279.

[9]     K. Celebi, T. D. Heidel, M. A. Baldo, *Opt. Express* **2007**, *15*, 1762.

[10]     J. Kim, H. Zhao, S. Hou, M. Khatoniar, V. Menon, S. R. Forrest, *Phys. Rev. Appl.* **2020**, *14*, 034048.

[11]     a) J. A. Kurvits, M. Jiang, R. Zia, *J. Opt. Soc. Am. A* **2015**, *32*, 2082; b) J. A. Schuller, S. Karaveli, T. Schiros, K. He, S. Yang, I. Kymissis, J. Shan, R. Zia, *Nat Nanotechnol* **2013**, *8*, 271; c) M. A. Lieb, J. M. Zavislan, L. Novotny, *J. Opt. Soc. Am. B* **2004**, *21*, 1210; d) T. H. Taminiau, F. D. Stefani, F. B. Segerink, N. F. van Hulst, *Nat. Photonics* **2008**, *2*, 234; e) M. Böhmler, N. Hartmann, C. Georgi, F. Hennrich, A. A. Green, M. C. Hersam, A. Hartschuh, *Opt. Express* **2010**, *18*, 16443.

[12]     S. R. Forrest, D. D. C. Bradley, M. E. Thompson, *Adv. Mater.* **2003**, *15*, 1043.

[13]     R. R. Chance, A. Prock, R. Silbey, *J.Chem.Phys.* **1974**, *60*, 2744.

[14]     A. Graf, P. Liehm, C. Murawski, S. Hofmann, K. Leo, M. C. Gather, *J. Mater. Chem. C* **2014**, *2*, 10298.

[15]     Y. Kawamura, H. Sasabe, C. Adachi, *Jap. J. Appl. Phys.* **2005**, *44*, 1160.